Conformational flexibility of the Cys 697–Cys 707 segment of myosin subfragment-1

ARTICLE *in* BIOPHYSICAL CHEMISTRY · MAY 1991

Impact Factor: 1.99 · DOI: 10.1016/0301-4622(91)85025-L

6 AUTHORS, INCLUDING:

Ignacy Gryczynski
University of North Texas HSC at F…
366 PUBLICATIONS **9,383** CITATIONS

SEE PROFILE

Joseph R Lakowicz
University of Maryland Medical Ce…
876 PUBLICATIONS **42,204** CITATIONS

SEE PROFILE

Biophysical Chemistry 40 (1991) 1–17
Elsevier Science Publishers B.V., Amsterdam

BIOCHE 01544

Conformational flexibility of the Cys 697-Cys 707 segment of myosin subfragment-1

Distance distributions by frequency-domain fluorometry

Herbert C. Cheung [a,*], Ignacy Gryczynski [b], Henryk Malak [b], Wieslaw Wiczk [b], Michael L. Johnson [c] and Joseph R. Lakowicz [b]

[a] *Department of Biochemistry, University of Alabama at Birmingham, University Station, Birmingham, AL 35294,* [b] *Center for Fluorescence Spectroscopy and Department of Biological Chemistry, School of Medicine, University of Maryland at Baltimore, Baltimore, MD 21201 and* [c] *Department of Pharmacology, University of Virginia, Charlottesville, VA 22908, U.S.A.*

Received 23 April 1990
Revised manuscript received 8 October 1990
Accepted 8 October 1990

Frequency-domain fluorometry; Myosin subfragment-1; Distance distribution; Anisotropy decay

The separation between Cys 697 (SH_1) and Cys 707 (SH_2) of the heavy chain of myosin subfragment-1 was previously measured by fluorescence resonance energy transfer with a donor linked to SH_1 and an acceptor to SH_2. In the present study the distribution of the distances between the two thiols was recovered from frequency-domain fluorometry. In the native state and in the presence of ligands such as MgADP, pyrophosphate, orthovanadate (V_i) and actin, we found wide distributions of the separations between SH_1 and SH_2 (11–16 Å) comparable to that found in the random-coil state (20 Å). These results suggest that the SH_1-SH_2 segment has a high degree of conformational flexibility even in native S1. The flexibility is not much affected by the physiological state of S1. However, the ligands MgADP, V_i and MgADP + V_i decrease significantly the mean SH_1-SH_2 distance from 27 to 17 Å with the effect of MgADP + V_i being the most pronounced. The anisotropy decay of donor-labeled S1 is biphasic with two rotational correlation times. The long component is decreased by these ligands from 289 to 93 ns, suggesting a more compact symmetric structure of S1 in the presence of the ligands. The complex S1 (MgADP)V_i has been shown to be a stable analogue of S1(MgADP)P_i, an unstable intermediate that is generated in the actomyosin ATPase cycle during muscle contraction. Since the power stroke of muscle is accompanied by release of P_i from S1(MgADP)P_i, the present results are consistent with a model in which force generation can be accompanied by transition of S1 from a highly symmetric or compact structure to a more extended structure.

1. Introduction

Several lines of evidence have made it increasingly clear that intersite communication within the myosin head (subfragment-1, S1) may be an important feature of energy transduction in muscular contraction [1,2]. The sites involved in the putative communication are the actin-binding sites and the ATPase site. Isolated S1 heavy chain is susceptible to tryptic digestion into three segments with molecular masses 27, 50, and 20 kDa starting from the N-terminus. In intact native S1 these segments appear to be contiguous at or near the ATPase site [2]. One can envision an 'energy transduction loop' within S1 in which molecular information is transmitted as a part of the transduction mechanism.

* To whom correspondence should be addressed.

Abbreviations: S1, myosin subfragment-1; AEDANS or IAEDANS, *N*-(iodoacetyl)-*N'*-(5-sulfo-1-naphthyl)ethylenediamine; DDPM, *N*-(4-dimethylamino-3,5-dinitrophenyl)maleimide; FRET, fluorescence resonance energy transfer; D-A, donor-acceptor.

0301-4622/91/$03.50

Within or close to the loop are located two residues (Cys 697 and Cys 707) which are located within the 20 kDa tryptic segment and can be easily and selectively alkylated. The SH_1-SH_2 region of the heavy chain may play a role in the communicaton process. Early studies showed that alkylation of the thiol SH_1 (Cys 707) activates the Ca-ATPase [3]. Subsequent modification of the other thiol SH_2 (Cys 697) in the presence of nucleotides completely abolishes the Ca-ATPase activity [4]. Chemical studies indicated that SH_1 and SH_2 can be cross-linked by a variety of bifunctional reagents with different spans from 12–14 Å [5] down to 3–5 Å [6]. These results suggest that the polypeptide backbone of S1 heavy chain between Cys 697 and Cys 707 is highly flexible. Recent studies [7,8] showed that the fluorescence resonance energy transfer between a donor (AEDANS) linked to SH_1 and an acceptor (DDPM) attached to SH_2 was significantly enhanced upon addition of MgADP, suggesting a decrease in the SH_1-SH_2 distance of 6–8 Å induced by the binding of the nucleotide. This decrease in distance was recently shown [9] to occur in two first-order kinetic steps with rate constants in the range 2–30 s^{-1}. The fast step is associated with a 4–5 Å decrease of the donor-acceptor distance, while the slow step is associated with with a further decrease of approx. 2 Å.

The amino acid sequence of S1 heavy chain between Cys 697 and Cys 707 is generally conserved from nonmuscle to muscle myosins. This sequence is in fact identical in rabbit skeletal, rabbit cardiac, chicken skeletal, and chicken smooth muscle myosins. Since in nonmuscle myosins Cys 697 or Cys 707 (or both) are replaced by other residues, the essential nature of the cysteine residues can be questioned. On the other hand, it is relevant to consider in what way the flexibility of this region of S1 heavy chain may play a role in energy transduction. To address this problem, it is important first to obtain direct confirmation of the extreme flexible nature of the Cys 697-Cys 707 segment that has been suggested by various lines of evidence.

Macromolecular flexibility arises from the intrinsic flexibility of the peptide and Brownian displacements due to thermal energy. The putative flexibility of the SH_1-SH_2 segment of S1 must reflect conformational heterogeneity and fluctuations in the 'end-to-end' distance of the segment between the two residues. In a series of recent papers [10,11], we have demonstrated the feasibility of recovering distributions of molecular distances in proteins by using frequency-domain fluorometry. This method of FRET and frequency-domain fluorometry was used in the present work to determine the distributions of the Cys 697-Cys 707 distances. The recovered distributions provide direct evidence that this segment in native S1 is highly flexible. Ligand binding at various sites does not significantly affect this flexibility but decreases the mean distance by up to 10 Å.

2. Theory

A detailed description of the basis for the recovery of distance distributions from frequency-domain FRET data has been published elsewhere [11]. A summary of the theory pertaining to the present work is given in this section.

If the fluorescence decay of a FRET donor in the absence of an acceptor is single-exponential with decay time τ_D, its intensity decay is given by

$$I_D(t) = I_D^0 \exp(-t/\tau_D) \tag{1}$$

If a single energy acceptor is located at a unique distance r from the donor, the donor decay is expected to remain a single-exponential with decay time $\tau_{DA} < \tau_D$. The intensity decay of the donor is then given by

$$\begin{aligned} I_{DA}(r, t) &= I_{DA}^0 \exp(-t/\tau_{DA}) \\ &= I_{DA}^0 \exp(-t/\tau_D - k_{DA}t) \end{aligned} \tag{2}$$

where R_0 is the Förster critical distance, and $k_{DA} = 1/\tau_D[R_0/r]^6$ is the rate of energy transfer, and τ_{DA} is related to τ_D and the donor-acceptor separation r by

$$\frac{1}{\tau_{DA}} = \frac{1}{\tau_D} + \frac{1}{\tau_D}\left[\frac{R_0}{r}\right]^6 \tag{3}$$

We note that in general $I_D^0 = I_{DA}^0$, i.e., the initial intensity of the donor and the donor-acceptor pair

will be identical. This is because these initial intensities refer to the same molecular species and because the absorption coefficient and radiative decay rate of the donor are assumed to be unaffected by the presence of acceptor. The transfer efficiency (E) can be related to the decay times using the time-integrated values of the intensity decays ($\bar{I}_D(t)$ or $\bar{I}_{DA}(t)$). Hence,

$$E = 1 - \frac{\bar{I}_{DA}}{\bar{I}_D} = 1 - \frac{\tau_{DA}}{\tau_D} = \frac{R_0^6}{R_0^6 + r^6} \tag{4}$$

If the single acceptor is not rigidly fixed in space with respect to the donor coordinates, there will be a range of donor-acceptor distances. While the decay of the donor corresponding to each donor-acceptor distance will still be a single-exponential, the overall observed donor decay will contain contributions reflecting the range of all possible donor-acceptor distances and is thus more complex than a single exponential. It is this deviation from single-exponential behavior that provides a measure of the donor-acceptor distance distribution. In this case, both the intensity decay of the donor in the presence of energy transfer and the transfer efficiency are each given by the average of the individual decays and transfer efficiencies weighted by the normalized distance probability distribution $P(r)$ of the donor-acceptor pair

$$I_{DA}(t) = I_{DA}^0 \int_0^\infty P(r) \exp(-t/\tau_{DA})\, dr \tag{5}$$

$$E = \int_0^\infty \frac{P(r) R_0^6\, dr}{R_0^6 + r^6} \tag{6}$$

In frequency-domain fluorometry, the measured quantities are the frequency-dependent phase shift (ϕ_ω) and modulation (m_ω). These values can be calculated from the sine (N_ω) and cosine (D_ω) transforms of the intensity decay function

$$\phi_{c\omega} = \arctan(N_\omega / D_\omega) \tag{7}$$

$$m_{c\omega} = \left(N_\omega^2 + D_\omega^2\right)^{1/2} \tag{8}$$

For a donor that decays monoexponentially in the absence of energy transfer and a donor-acceptor pair that can be characterized by a probability distribution of donor-acceptor distances, the two transforms are given by [12]

$$N_\omega^{DA} = \frac{1}{J_{DA}} \int_0^\infty \frac{P(r)\, \omega \tau_{DA}^2}{1 + \omega^2 \tau_{DA}^2} dr \tag{9}$$

$$D_\omega^{DA} = \frac{1}{J_{DA}} \int_0^\infty \frac{P(r)\, \tau_{DA}}{1 + \omega^2 \tau_{DA}^2} dr \tag{10}$$

where J_{DA} is a normalization factor and is given by

$$J_{DA} = \int_0^\infty P(r)\, dr \int_0^\infty I_{DA}(t)\, dt$$

$$= \int_0^\infty P(r)\, \tau_{DA}\, dr \tag{11}$$

These transforms can be calculated numerically. In practice the range of distances of the integrals is from a minimum distance r_{min} near 5 Å to a maximum distance r_{max} near 50 Å. The recovered distance distributions are not sensitive to the precise value of r_{min} and r_{max} as long as the range is adequate to account for the experimental data.

If the donor decay in the absence of energy transfer is multiexponential, then eqs 1 and 5 will be sums of exponential terms

$$I_D(t) = I_D^0 \sum_i \alpha_{Di} \exp(-t/\tau_{Di}) \tag{12}$$

$$I_{DA}(t) = I_{DA}^0 \int_0^\infty P(r) \sum_i \alpha_{Di} \times \exp\left[-\frac{t}{\tau_{Di}} - \frac{t}{\tau_{Di}} \left(\frac{R_0}{r} \right)^6 \right] dr \tag{13}$$

where α_{Di} are the pre-exponential factors and τ_{Di} the associated decay times in the absence of acceptor (energy transfer),

$$\frac{1}{\tau_{DAi}} = \frac{1}{\tau_{Di}} + \frac{1}{\tau_{Di}} \left(\frac{R_0}{r} \right)^6 \tag{14}$$

The sine and cosine transforms of the intensity

decay function weighted by the probability distribution $P(r)$ are

$$N_\omega^{DA} = \frac{1}{J_{DA}} \int_0^\infty \sum_i \frac{P(r)\alpha_{Di}\omega\tau_{DAi}^2}{1+\omega^2\tau_{DAi}^2} dr \quad (15)$$

$$D_\omega^{DA} = \frac{1}{J_{DA}} \int_0^\infty \sum_i \frac{P(r)\alpha_{Di}\tau_{DAi}}{1+\omega^2\tau_{DAi}^2} dr \quad (16)$$

$$J^{DA} = \int_0^\infty \sum_i P(r)\alpha_{Di}\tau_{DAi}\, dr \quad (17)$$

The parameters describing the intensity decay (eq. 5 or eq. 13) and the probability distribution $P(r)$ can be estimated from the experimental (ϕ_ω and m_ω) and calculated ($\phi_{c\omega}$ and $m_{c\omega}$) values of the phase shift and the modulation by using a nonlinear least-squares procedure [13] in which the chi-square ratio is minimized

$$\chi_R^2 = \frac{1}{\nu}\sum_\omega \frac{(\phi_\omega - \phi_{c\omega})^2}{\delta\phi} + \frac{1}{\nu}\sum_\omega \frac{(m_\omega - m_{c\omega})^2}{\delta m} \quad (18)$$

where ν is the number of degrees of freedom and $\delta\phi$ and δm denote the experimental uncertainties in the measured phase and modulation values. For the present study a Gaussian function was used as the probability distribution of donor-acceptor distances

$$P(r) = \frac{1}{\sigma\sqrt{2\pi}} \exp\left[-\frac{1}{2}\left(\frac{r-\bar{r}}{\sigma}\right)^2\right] \quad (19)$$

where $\bar{r}$ is the mean distance and σ represents the standard deviation of the untruncated Gaussian. The standard deviation is related to the half-width (hw, full width at half-maximum height) by hw = 2.354σ. Outside the interval between r_{min} and r_{max} the probability $P(r)$ is set equal to zero. Depending upon the values of r and hw the distance-integrated value of $P(r)$ may be less than unity. This occurs when part of the distribution occurs below $r = 0$. The integral in eq. 17 normalizes $P(r)$ and corrects for this missing part of the distribution. In practice, the integration is performed over a limited range, from about 5 Å to 3–5-times the Förster distance. In general, the results of the analyses are unaffected by the chosen limits. For calculation of χ_R^2, and for simulations of experimental data, the uncertainties in the phase ($\delta\phi$) and modulation (δm) were taken as 0.2^0 and 0.005, respectively.

Suppose the donor-to-acceptor separation is characterized by a single distance r. It is interesting to note the relationship between the intensity decay parameters (α_{Di} and τ_{DAi}) and the transfer efficiency. Integration of eqs 12 and 13 over time and eq. 4 yields

$$E = 1 - \frac{\bar{I}_{DA}}{\bar{I}_D} = 1 - \frac{\sum_i \alpha_{Di}\tau_{DAi}}{\sum_i \alpha_{Di}\tau_{Di}} \quad (20)$$

To be more explicit, use of eq. 3 with the decay times is only valid if the decay is a single-exponential, and there is a single donor-to-acceptor distance. If the decays of the donor or donor-acceptor pair are multiexponential, or if there exist multiple D-A distances, then calculation of the transfer efficiency requires use of the relative quantum yields, which are given by the sum of the $\alpha_i\tau_i$ products.

3. Experimental

3.1. Frequency-domain measurements

Fluorescence lifetimes were determined from the frequency response of the emission using the instrument previously described by Lakowicz et al. [14]. The cavity-dumped output of a synchronously pumped pyridine 2 dye laser was used to generate a laser pulse train with a repetition rate of 3.79 MHz and a pulse width of about 5 ps, which was then frequency-doubled to 355 nm. This source is intrinsically modulated to many gigahertz and used to excite directly the samples. The intensity decays were measured using rotation-free magic angle polarized conditions. The donor emission was isolated by a 480-nm interference filter and detected by a Hamamatsu R1564U microchannel plate photomultiplier tube, which allows detection of the modulated emission to 2 GHz [14].

3.2. Correction for incomplete labeling by acceptor

In the determination of distance distributions it is critical to know the extent of labeling with the acceptor; the extent of donor labeling is less critical. If the acceptor is present at a fractional labeling (L) of 1.0, and the donor labeling is less than unity, all the donor-labeled molecules participate in energy transfer. Since we are using the donor decay, the results are unaffected by incomplete donor labeling. In contrast, if the extent of acceptor labeling is less than 1.0 then some of the donors do not have a nearby acceptor. These acceptor-free donor molecules are unquenched by energy transfer, and hence the observed donor emission contains a component which is unaffected by energy transfer. Additionally, these acceptor-free donors contribute to the observed fluorescence in excess of their molar proportion because of their higher relative quantum yield. In order to calculate the distance distributions one must correct for this nonstoichiometric labeling (under labeling) of the protein by acceptor. For this correction we assume that the observed intensity decay of the donor results from the emission of the donor alone [$I_D(t)$] and from the emission of the D-A pairs [$I_{DA}(t)$], weighted by the relative proportion of each species in the sample. The observed intensity is given by

$$I_{obs}(t) = (1-L)I_D(t) + L \cdot I_{DA}(t) \tag{21}$$

$$I_{obs}(t) = (1-L)I_D^0 \sum_i \alpha_{Di} \exp(-t/\tau_{Di}) + L \cdot I_{DA}^0 \int_0^\infty P(r) \sum_i \alpha_{Di} \times \exp\left[-\frac{t}{\tau_{Di}} - \frac{t}{\tau_{Di}}\left(\frac{R_0}{r}\right)^6\right] dr \tag{22}$$

In this last expression we used equivalent values of I_D^0 and I_{DA}^0. One observes in eqs 21 and 22 that the donor-alone molecules contribute in excess of their molar proportion due to the higher relative intensity of $I_D^0(t)$ vs $I_{DA}^0(t)$. In our procedure the extent of labeling (L) can be determined by varying L to yield the minimum value of χ_R^2. Once this was done for a given preparation, L was held constant in all subsequent analyses. Alternatively, the extent of labeling can be determined by chemical and/or spectroscopic analysis of the samples. In the present paper the extent of labeling was found to be 0.96 by absorbance measurements and 0.94 from the χ_R^2 minimum. The value of L was held fixed at this latter value for all analyses.

3.3. Frequency-domain expressions with incomplete labeling

A complete description of the procedure to correct for incomplete labeling, along with an experimental verification of the procedure, will be published elsewhere [15]. The frequency-domain expressions for the observed emission are

$$N_\omega^{obs} = \frac{1}{J_{obs}}\left[(1-L)J^D N_\omega^D + LJ^{DA}N_\omega^{DA}\right] \tag{23}$$

$$D_\omega^{obs} = \frac{1}{J_{obs}}\left[(1-L)J^D D_\omega^D + LJ^{DA}D_\omega^{DA}\right] \tag{24}$$

$$J^{obs} = (1-L)J^D + LJ^{DA} \tag{25}$$

where N_ω^{DA}, D_ω^{DA}, and J^{DA} are given by eqs 15–17,

$$N_\omega^D = \frac{1}{J^D}\sum_i \frac{\omega \alpha_{Di}\tau_{Di}^2}{1+\omega^2\tau_{Di}^2} \tag{26}$$

$$D_\omega^D = \frac{1}{J^D}\sum_i \frac{\alpha_{Di}\tau_{Di}}{1+\omega^2\tau_{Di}^2} \tag{27}$$

$$J^D = \sum_i \alpha_{Di}\tau_{Di} \tag{28}$$

3.4. Anisotropy decays

Anistropy decays were obtained from the frequency response of the polarized emission [16]. The data were fitted to a biexponential decay law

$$r(t) = r_0 \sum_i g_i \exp(-t/\theta_i) \tag{29}$$

where r_0 is the limiting anisotropy in the absence of rotational motions, θ_i denote the rotational correlation times, and g_i the associated amplitudes. In our analyses the total anisotropy was taken as a variable parameter, so that the amplitudes were obtained as values for $r_0 g_i = r_{0i}$.

3.5. Protein preparations and chemicals

Myosin was prepared from rabbit skeletal muscle as previously described [17]. Myosin subfragment-1 was obtained by digestion of myosin with chymotrypsin, followed by purification on a DEAE-cellulose (DE 52) column as described by Weeds and Taylor [18]. The two isozymes S1(A1) and S1(A2) were pooled for subsequent labeling with fluorescent probes. Actin was prepared from an acetone powder according to Spudich and Watts [19] and polymerized as described previously [20]. Polymerized actin was extensively dialyzed against 60 mM KCl and 30 mM Tes at pH 7.5 for 24 h and used immediately to obtain actosubfragment-1. The modification of SH_1 by AEDANS and SH_2 by DDPM was carried out using the same procedure as in our earlier work [8]. The degree of SH_1 and SH_2 labeling was determined by absorbance measurements [8]. The degree of acceptor labeling was found to be 0.96 from the absorbance.

The concentration of S1 was estimated from an absorbance of 0.75 $g^{-1}\,cm^{-1}$ at 280 nm [21] and a molecular weight of 115 000. An absorbance of 0.63 $g^{-1}\,cm^{-1}$ at 290 nm [22] and a molecular weight of 42 000 were used to determine the concentration of actin. IAEDANS was purchased from Molecular Probes (Eugene, OR) and DDPM from Aldrich Chemicals (Milwaukee, WI). V_2O_5 obtained from Aldrich Chemicals was used to prepare a stock solution of sodium vanadate (V_i) as previously described [17]. All other chemicals were of reagent grade.

4. Results

4.1. Simulation of distance distributions

Simulated data which demonstrate the sensitivity of the frequency-domain data to the width of Gaussian-distributed donor-acceptor distances are shown in fig. 1. A single donor decay time (τ_D) of 20 ns and a value of 30 Å for R_0 were used in the simulations. These values are comparable to the experimental values of the S1 system reported in this paper. For the simulations we used 30 frequencies in the range 3–300 MHz. The data contain random noise of a level comparable to our experimental data (0.2° in phase and 0.005 in modulation). In fig. 1A the half-width (hw) of the distribution is assumed to be 1.0 Å, which is equivalent to a single donor-acceptor distance. The simulated data are well-fitted to a single-exponential decay. When hw is increased by 15-fold to 15.0 Å (fig. 1B), the simulated data clearly are not compatible with a single-exponential model. The large deviation from single exponentiality is a consequence of the substantial broadening of the distribution function and reflects the presence of a range of donor-acceptor distances. A half-width of 15 Å corresponds to considerable heterogeneity in the donor-acceptor distances and such a broad

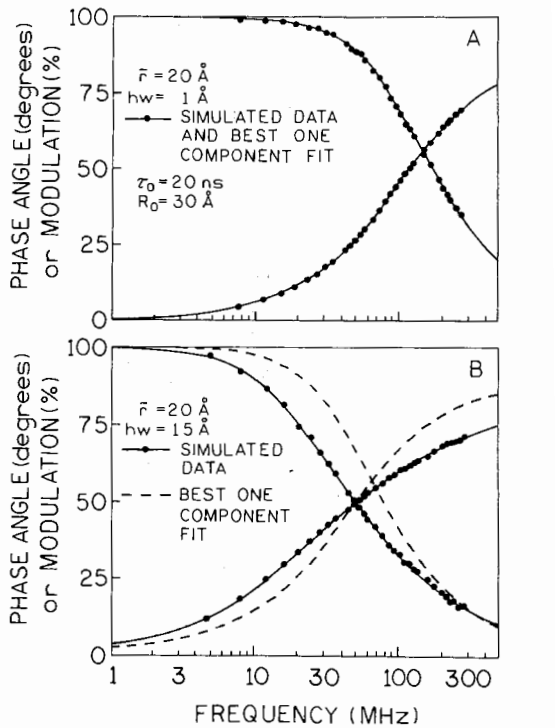

Fig. 1. Simulated frequency response for a donor-acceptor pair with $\tau_D = 20$ ns, $R_0 = 30$ Å, $\bar{r} = 20$ Å. The phase angles increase and the modulation decreases with increasing frequency. (Upper panel) Gaussian distribution with half-width (hw) = 1 Å is used in the simulation. The solid curves are the best single-exponential fits to the simulated values (●). (Lower panel) hw is 15 Å. The dashed curves are the best single-exponential fits to the simulated data (●), and the solid curve is the best fit using the distance distribution model.

distribution is easily detected from frequency-domain measurements.

For smaller increases in hw, the departure from single-exponentiality is less pronounced than that displayed in fig. 1B and may not be graphically discernible. However, these smaller deviations can be revealed from an examination of the χ^2_R ratio for the fitting of the phase shift and modulation values to a monoexponential model of donor decay. These results are given in table 1. For hw = 1.0 Å the simulated data are very satisfactorily fitted to a single donor decay time (fig. 1A) with $\chi^2_R = 0.7$. If the same set of data are fitted to a distribution using a fixed incorrect value of 3.0 Å for hw, the χ^2_R value is 22; and if hw is fixed at 6.0 Å, χ^2_R is 238. This result demonstrates that a narrow distribution of D-to-A distances can be resolved. Importantly, if the donor-to-acceptor distribution is in fact narrow (i.e., about 1 Å), the measurements and analysis will not report a distribution wider than 1 Å due to limited experimental resolution. If the correct width is 15.0 Å, χ^2_R increases by a factor of 35–90 when the data are fitted to incorrect widths of 10.0 or 20.0 Å. If the hw is fixed at 1.0, χ^2_R is elevated to 993. Thus, the statistical parameter χ^2_R is a sufficiently sensitive criterion to judge the existence of a distribution of FRET distances, and to reveal the width of these distributions. While the simulations are for monoexponential donor decay, similar results were obtained for donor decays which follow a multiple-exponential decay law. Our theory and algorithm do not require that the donor decay be a single-exponential [11].

Table 1

Sensitivity of χ^2_R to changes in the half-width of the distance distribution

Input value		Calculated values		χ^2_R
$\bar{r}$ (Å)	hw[a] (Å)	$\bar{r}$ (Å)	hw (Å)	
20	1.0	20.0	1.06	0.7 [c]
		19.8	⟨3.0⟩ [b]	22.2
		19.8	⟨6.0⟩	238.2
		12.2	⟨15.0⟩	1463.7
20	15.0	20.0	15.1	1.2
		22.1	⟨10.0⟩	106.6
		16.8	⟨20.0⟩	40.5
		28.7	⟨1.0⟩	992.7

[a] hw is the full width at half maximum height for a Gaussian distribution.

[b] ⟨ ⟩ indicates that hw was held fixed at the indicated value during least-squares analysis.

[c] The χ^2_R values were obtained in least-squares analysis using $\delta\phi = 0.2°$ and $\delta m = 0.005$.

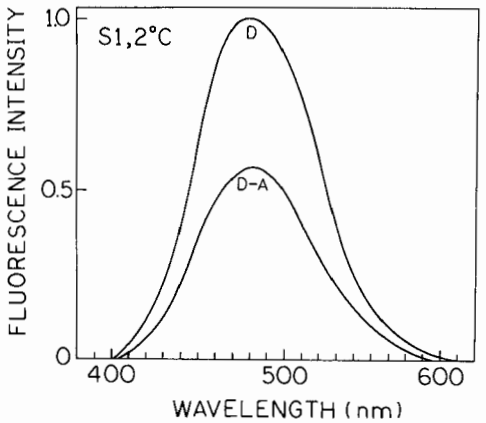

Fig. 2. Fluorescence spectra of donor-labeled S1 (D) and S1 labeled with both donor and acceptor (D-A). The donor was AEDANS attached to Cys 707 and the acceptor was DDPM linked to Cys 697.

4.2. Emission of AEDANS-S1

The emission spectra of donor (AEDANS)-labeled S1 and S1 labeled with both donor and acceptor (DDPM) are shown in fig. 2. The large decrease in intensity due to the presence of the acceptor provides evidence of energy transfer. However, the steady-state data can only yield an average distance between the D-A pair, and cannot provide the distance distribution unless one synthesizes several labeled proteins, each with a different donor-acceptor pair which has a different value of R_0 [23,24]. In contrast, the distance distribution can be recovered from a single D-A pair if one can recover the time-resolved decay of the donor.

We recover the time-resolved donor decay from its frequency response. The frequency response of donor and donor-plus-acceptor labeled S1 was studied under a variety of conditions. Shown in fig. 3 are the changes of the phase angle and modulation as a function of frequency for donor-

Table 2

Intensity decay parameters for myosin subfragment-1 labeled at Cys 707 (SH_1) with AEDANS

Conditions [a]	τ_i (ns)	α_i	f_i [b]	$\bar{\tau}_D$ [c] (ns)	χ^2_R
Buffer	18.40	1.0	1.0		82.4
	4.02	0.181	0.040		
	21.36	0.819	0.960	20.67	1.7
MgADP	18.41	1.0	1.0		69.4
	4.01	0.168	0.037		
	21.13	0.832	0.963	20.50	1.9
Pyrophosphate	18.40	1.0	1.0		93.9
	2.35	0.180	0.035		
	21.46	0.820	0.965	20.83	1.4
Vanadate	18.83	1.0	1.0		68.8
	3.5	0.153	0.029		
	21.17	0.847	0.971	20.65	1.9
MgADP + vanadate	19.76	1.0	1.0		85.0
	3.93	0.174	0.035		
	22.61	0.826	0.965	21.96	1.4
Actin	18.56	1.0	1.0		97.1
	2.41	0.185	0.021		
	20.91	0.842	0.978	20.52	1.6
Gdn·HCl	11.14	1.0	1.0		172.6
	4.26	0.369	0.140		
	15.14	0.631	0.860	13.60	2.7

[a] All samples were in 60 mM KCl, 30 mM Tes (pH 7.5). For the first five samples, the S1 concentration was in the range of 25–30 μM; where applicable, $MgCl_2$ was 1 mM, ADP 100 mM, sodium pyrophosphate 150 μM, and vanadate 1 mM. The last two samples contained 17.4 μM S1 and either 47 μM actin or 6 M Gdn·HCl. All measurements were made at 2° C, with an excitation wavelength of 355 nm. Each set of decay data was fitted to a one-exponential and a two-exponential function. The results shown for buffer, MgADP, vanadate and MgADP + vanadate represent an average of two separate experiments, yielding very similar results.

[b] Fractional intensity f_i was calculated from

$$f_i = \alpha_i\tau_i / \sum \alpha_i\tau_i, \text{ with } \sum f_i = 1.0$$

[c] Mean donor lifetime was calculated from $\bar{\tau}_D = \Sigma f_i\tau_i$

labeled S1 and S1 labeled with donor and acceptor determined in the presence of MgADP. It is clear that the decay was not monoexponential for both samples. The deviation from single-exponential decay was substantial even for the donor-labeled sample, and larger for the sample containing both donor and acceptor. The increased heterogeneity of the donor decay in the presence of acceptor is due to the distribution of D-to-A distances, which in turn results in a distribution of rates for energy transfer.

The decay data for donor-labeled S1 are summarized in table 2. Each set of the decay data could be fitted with a biexponential function. No improvement in the fitting was obtained when the data were fitted to a three-exponential model. In the native protein the short decay component contributed 4% or less to the total emission with the weighted average of the decay times being about 21 ns. The average lifetime was little affected by the presence of various ligands and increased by about 1 ns when S1 was complexed to actin. In the presence of 6 M guanidine hydrochloride the average lifetime was reduced by 33% to 13.6 ns, and the contribution of the shorter decay time increased to 14%.

Table 3

Typical multiexponential analysis of intensity decays of myosin subfragment-1 labeled with both donor and acceptor

Conditions [a]	τ_i (ns)	α_i	f_i	$\bar{\tau}_{DA}$(ns)	χ^2_R		
					1 [b]	2	3
Buffer	1.76	0.269	0.056	12.39			
	6.31	0.394	0.296				
	16.10	0.337	0.648		465.8	5.8	1.7
MgADP	0.88	0.447	0.086	10.29			
	4.49	0.418	0.414				
	16.75	0.135	0.500		1389.4	46.5	2.1
Pyrophosphate	1.74	0.359	0.092	11.16			
	6.36	0.433	0.406				
	16.37	0.208	0.502		618.4	8.3	1.5
Vanadate	1.42	0.143	0.016	17.12			
	5.49	0.256	0.108				
	18.84	0.601	0.876		291.4	4.5	2.4
MgADP+vanadate	2.02	0.359	0.059	18.75			
	9.27	0.241	0.182				
	22.32	0.400	0.759		767.4	6.0	1.2
Actin	1.34	0.240	0.035	13.01			
	6.49	0.291	0.204				
	15.04	0.469	0.761		353.8	5.6	2.2
Gdn·HCl	0.90	0.402	0.080	8.63			
	3.66	0.362	0.293				
	11.94	0.237	0.627		1034.7	9.4	2.3

[a] Sample conditions were the same as listed in table 2. The results shown are for three-component fits.

[b] The χ^2_R values for one-component (1), two-component (2), and three-component (3) fits are given in the last three columns under χ^2_R.

The decay data of S1 labeled with both donor and acceptor were fitted with monoexponential, biexponential, and triexponential models. A typical set of these results are listed in table 3. In every case the best fit was obtained with a three-exponential model and the average lifetime ($\bar{\tau}_{DA}$) was considerably reduced from that of the donor itself (τ_D). Since the donor decay (in the absence of acceptor) followed a biexponential decay law, the departure of the decay in the presence of acceptor from a biexponential model provides evidence that the D-A separation cannot be represented by a single distance.

4.3. Anisotropy decays of donor-labeled S1

The anisotropy decays of AEDANS-S1 were measured in the absence and presence of several ligands and guanidine hydrochloride. A typical set of anisotropy data is shown in fig. 4. The frequency distributions of the differential phase angles were non-Lorentzian for all conditions studied, indicating the presence of more than a single rotational correlation time. The differential polarized phase and modulated anisotropy data could be adequately fitted with two correlation times. These results are listed in table 4. In the absence of bound ligands, 22% of the total anisotropy decayed with a short correlation time of 9.5 ns and the remainder with a long correlation time of 289 ns. The presence of various ligands did not alter the total anisotropy, but reduced the contribution associated with the short correlation time by a factor of 1.2–3.8, to about 10% of the total anisotropy. The constant value of $r_0 = r_0 g_1 + r_0 g_2$ and the constant limiting value of the modulated ani-

sotropy at high frequencies suggest that all of the fundamental anisotropy of the probe is recovered from the data [16]. Denaturation of S1 reduced the total anisotropy by 14% and shifted the major contribution to the short component. The decreased apparent value of $r_0 = r_0 g_1 + r_0 g_2$ suggests the presence of a rapid component in the anisotropy decay which is not recovered from the data.

The two correlation times were substantially reduced by all ligands studied. To determine the extent to which the ligand-induced changes were statistically significant, we examined the χ^2_R surfaces for the two correlation times (fig. 5). The surfaces were calculated by holding one correlation time constant at the values indicated on the horizontal axis and allowing the other correlation time and both amplitudes to vary so as to minimize χ^2_R. In these calculations the ranges of both θ_1 and θ_2 that are consistent with the data are

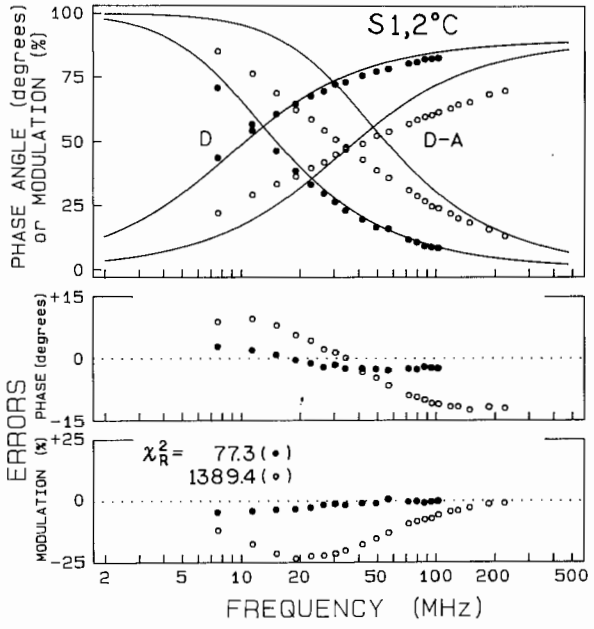

Fig. 3. Frequency response of AEDANS-labeled S1, in the absence (●, D) and presence (○, D-A) of DDPM acceptor. The frequency response of the D-A pair is shifted to the right due to energy transfer. The solid curves show the best fit of the observed data to a single decay time. The middle and bottom panels show the deviation between the data and the best single decay time fits.

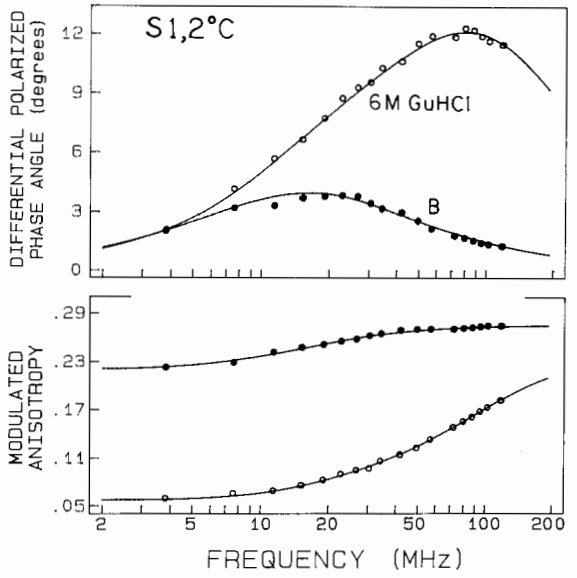

Fig. 4. Differential polarized phase angle data (top panel) and modulated anisotropy (lower panel) for S1 labeled with AEDANS: in standard buffer (●) and in 6 M guanidine hydrochloride (○).

given approximately by the range of values for which χ^2_R is elevated to the extent possible of 67% of the time due to random error. The short correlation time was significantly reduced by MgADP and denaturation of the protein by guanidine-

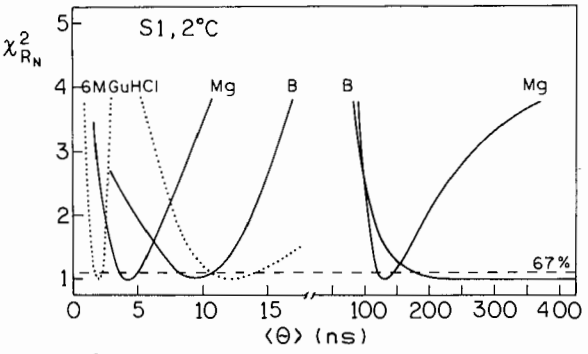

Fig. 5. χ^2_R surfaces for the two rotational correlation times calculated from anisotropy decay analysis of S1 labeled with AEDANS. (Left panel) (·····) for θ_1 and θ_2 determined in guanidine hydrochloride; (———) for θ_1 determined in buffer (B) and $MgCl_2$ (Mg). (Right panel) θ_2 determined in buffer (B) and $MgCl_2$ (Mg). The dashed horizontal line shows the upper value of χ^2_R consistent with the χ^2_R being due to random error in 67% of repetitive measurements.

Table 4

Anisotropy decays of AEDANS-Cys 707 in myosin subfragment-1

Conditions [a]	θ_i(ns) [b]	g_i	$g_i r_0$ [c]	χ^2_R
Buffer	64.8	1.0	0.270	29.9
	9.5	0.224	0.062	
	288.7	0.776	0.215	1.2
MgADP	77.4	1.0	0.272	19.6
	4.4	0.103	0.029	
	134.1	0.897	0.253	1.4
Pyrophosphate	68.2	1.0	0.263	32.7
	5.6	0.183	0.042	
	178.5	0.817	0.230	2.3
Vanadate	70.7	1.0	0.271	27.3
	5.6	0.136	0.038	
	152.1	0.864	0.242	1.6
MgADP + vanadate	73.5	1.0	0.274	3.6
	7.9	0.058	0.016	
	92.9	0.942	0.261	1.1
Gdn·HCl	3.5	1.0	0.217	23.0
	2.1	0.736	0.176	
	12.3	0.264	0.063	0.9

[a] Sample conditions were the same as listed in table 2; λ_{ex} = 355nm, λ_{em} = 480nm. The results shown for buffer, MgADP, vanadate and MgADP + vanadate represent an average of two separate experiments, yielding very similar results.

[b] The first number for each condition was from a one-exponential fit and the other two numbers were obtained from a biexponential fit.

[c] In our analysis the total anisotropy was taken as a variable parameter.

HCl. The χ^2_R surface for the long correlation time, in the absence of MgADP, indicates we are unable to resolve the longer correlation time. However, the calculations suggested that for this sample $\theta_2 > 175$ ns. In spite of this lack of resolution, it appears that θ_2 was significantly reduced by MgADP. A further decrease (30%) in θ_2 was observed upon addition of vanadate to the S1 · MgADP complex.

4.4. Distribution of D-A distances in S1

In order to recover distance distributions it is necessary to obtain the frequency-response of the donor in the presence of acceptor. It is frequently impossible with biochemical samples to obtain complete labeling with acceptor. Consequently, it is necessary to correct for the donor emission which is due to donor molecules without acceptors. This is accomplished using the distance distribution analysis with a component in the donor decay of the D-A pair which is the same as the donor-alone decay. The fractional labeling is varied to obtain the minimum value of χ^2_R (fig. 6). The fractional acceptor labeling of 0.94 is in excellent agreement with that obtained from the absorbance data.

The intensity decays of the donor and donor-acceptor pairs can be used to recover the distance distribution under a variety of experimental conditions. The multiexponential analyses listed in tables 2 and 3 can be considered to be parameterized forms of the donor decays. It is possible to analyze these multiexponential parameters, or the mean decay times, in terms of the distance distributions [25]. However, we prefer to avoid the intermediate step, and to analyze the frequency response directly in terms of the distance distribution. A typical analysis is shown in fig. 7 for the distribution recovered in the presence of MgADP.

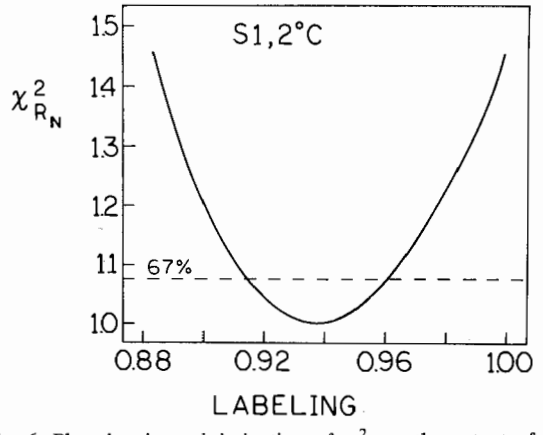

Fig. 6. Plot showing minimization of χ^2_R on the extent of S1 labeling by the acceptor DDPM. The hw and $\bar{r}$ were both variable parameters as the degree of labeling L was varied so as to obtain the minimum value of χ^2_R. The degree of labeling determined from this plot is 0.94 as compared with a value of 0.96 determined from absorbance measurements. The dashed horizontal line shows the upper value of χ^2_R consistent with the χ^2_R being due to random error in 67% of repetitive measurements. The values of χ^2_R are normalized (χ^2_{RN}) to the lowest value of χ^2_R.

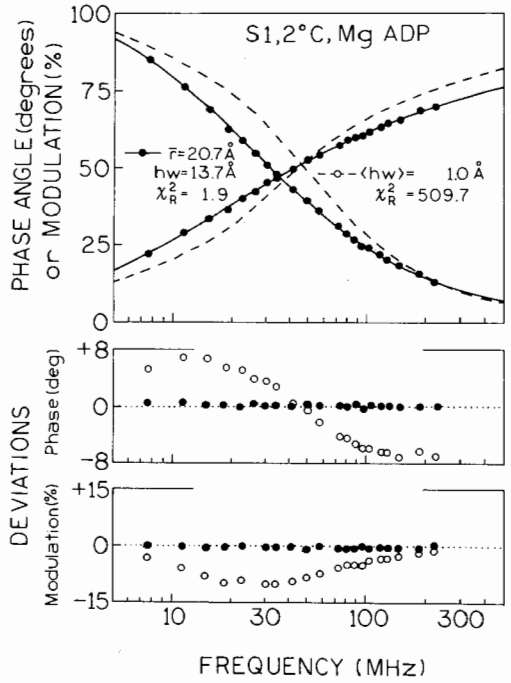

Fig. 7. Distance distribution analysis of the frequency-responses of donor and acceptor-labeled S1 in the presence of MgADP. The solid lines represent the best fits to the data using the Gaussian distance distribution model. This analysis yields $\bar{r} = 20.7$ Å and hw = 13.7 Å, $\chi^2_R = 1.9$. The dashed lines were obtained when the data were forced fitted to a narrow distribution with hw = 1 Å ($\chi^2_R = 509.7$).

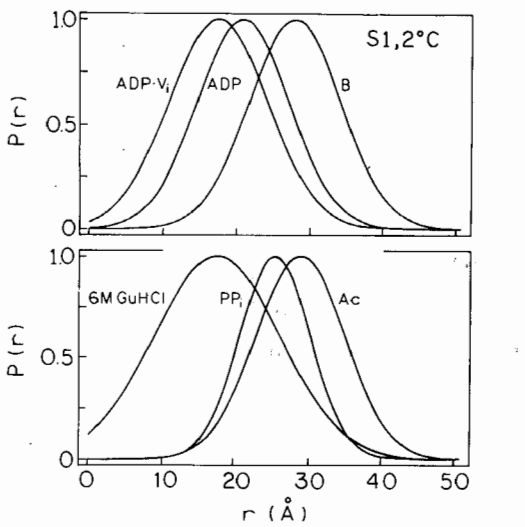

Fig. 8. Distributions of distances from Cys 707 to Cys 697. (Upper panel) donor and acceptor-labeled S1 in buffer (B), MgADP (ADP), and MgADP + V_i (ADP·V_i). (Lower panel) S1 in the presence of actin (Ac), pyrophosphate (PP_i), and guanidine hydrochloride (GuHCl).

For this sample the best fit yielded the following parameters: $\bar{r} = 20.7$ Å and hw = 13.7 Å with χ^2_R of 1.9. When the same set of data were refitted with hw fixed to 1 Å corresponding to a narrow distribution, the χ^2_R value increased by 300-fold to 509.7, indicating that the data were incompatible with a narrow range of distances. Fig. 8 shows the recovered distance distributions $P(r)$ for S1 in the presence of a variety of ligands and actin. The best fitted parameters characterizing the various distributions are listed in table 5. As for S1 alone, the data obtained in the presence of the various ligands could not be fitted to a narrow distribution of distances. The mean distance $\bar{r}$ was decreased from 27.3 to 20.7 Å by MgADP with a very small narrowing of $P(r)$. In the presence of pyrophosphate, $P(r)$ was also shifted toward shorter distances. Vanadate induced a decrease in $\bar{r}$ by about 1 Å, but MgADP and vanadate together reduced $\bar{r}$ to 17.2 Å. With the exception of pyrophosphate, these ligands induced a small or negligible broadening (1 Å) of the distributions. The presence of actin caused a small shift of $P(r)$ toward longer distances with a negligible effect on the hw. Denaturation of the protein resulted in a shift of $P(r)$ toward shorter distances and a broadening of the distribution by 5.6 Å.

Table 5

Distance distribution between Cys 697 and Cys 707 in myosin subfragment-1

Conditions [a]	R_0 (Å)	$\bar{r}$ (Å) [b]	hw(Å)	χ^2_R
Buffer	29.3	27.3	14.1	1.9
MgADP	29.3	20.7	13.7	1.9
Pyrophosphate	29.3	25.0	11.1	2.6
Vanadate	25.9	25.9	15.4	2.1
MgADP + vanadate	25.2	17.2	15.5	1.2
Actin	28.6	28.4	14.0	3.6
Gdn·HCl	24.3	17.2	19.7	2.0

[a] Sample conditions were the same as listed in table 2. The results shown for buffer, MgADP, vanadate and MgADP + vanadate represent an average of two separate experiments, yielding very similar results.

[b] The extent of acceptor labeling was held fixed at $L = 0.94$.

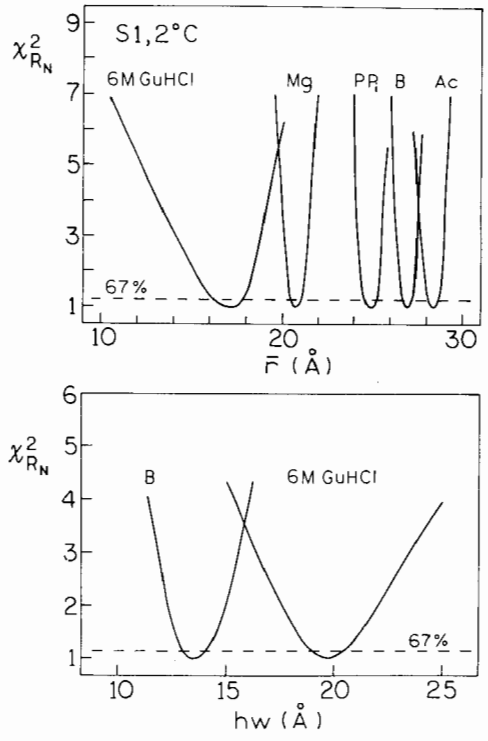

Fig. 9. Dependence of χ^2_R on the mean distances $\bar{r}$ and the half-widths (hw) of the D-A distributions in S1. (Top panel) The dependence on $\bar{r}$ in the presence of actin (Ac), buffer (B), pyrophosphate (PPi), MgADP (Mg), and guanidine hydrochloride (GuHCl). (Bottom panel) The dependence on hw in the presence of guanidine hydrochloride (right) and buffer (left). The horizontal dashed lines indicate the largest value of χ^2_R consistent with the value of χ^2_R being due to random noise in 67% of repetitive measurements.

It was of interest to examine the extent to which the various recovered distributions can be distinguished from one another. This was accomplished by examining the χ^2_R surfaces for $\bar{r}$ and hw as shown in fig. 9 for several cases. It is clear that all five distributions had significantly different $\bar{r}$ values. Fig. 9 also shows that the 45% increase in hw upon denaturation was significant. The range of hw for the denatured sample was 19.0–20.5 Å.

Finally, we considered the effect of the orientation factor κ^2 on the widths of the recovered distributions. This effect is difficult to evaluate because the precise value of κ^2 is unknown. There are two approaches to this problem. The approach of Dale et al. [26] to estimate the maximum and minimum values of κ^2 (and hence FRET distances) requires measurements of both donor and acceptor depolarization factors. Since the acceptor DDPM is not fluorescent, its depolarization factor cannot be determined. An alternate approach is based on the knowledge that the donor AEDANS has multiple transition dipole moments as reflected in its anisotropy spectrum. Haas et al. [27] have shown that the presence of such multiple transition moments should result in a smaller range of distances arising from orientation effects. These effects can be evaluated from the zero time anisotropy $r(0)$. The fact that no $r(0)$ value is available for the acceptor does not prevent us from estimating the maximum possible error introduced by a mobile acceptor. Using an $r(0)$ value of 0.270 for the donor AEDANS and an assumed value of 0.4 for the acceptor DDPM, we obtained from Haas et al. [27] a maximum range of distances for this donor-acceptor pair from 0.83 to 1.19 of the apparent single mean distance ($\bar{r}$). $\bar{r}$ was 27.3 Å in the absence of ligands and 20.7 Å in the presence of MgADP. The corresponding maximum ranges were thus 22.6–32.1 and 17.1–24.6 Å with maximum widths of 9.5 and 7.5 Å, respectively. The widths would be slightly reduced if the zero time anisotropy of the acceptor is comparable to that of the donor. Also, the range of apparent distances and widths due to orientation effects would be decreased further if we considered the rapid component in the anisotropy decay as described by Dale et al. [26]. Hence, the observed widths were in the range of 11–20 Å and are too large to be explained by the uncertainty in the orientation factor.

5. Discussion

The lifetime of AEDANS attached to Cys 707 (SH_1) of myosin subfragment 1 has been previously determined to be reasonably single-exponential with a value of about 20 ns [20,28]. The result was obtained by the time-domain pulse technique. In the present study we used the multifrequency method and found the decay to be biexponential with a minor short component. The fractional

intensity of this component varies from less than 1% to no more than 4%. While the origin of the minor component is unclear, it should be noted that the multifrequency method is more sensitive to the presence of a minor component with a short lifetime. The best weighted average of the two lifetimes is 20.67 ns at 2°C, in excellent agreement with the single lifetime determined by the time-domain method and reported by different laboratories. The present anisotropy decay data show two rotational correlation times and differ from previous results obtained by the time-domain technique which yielded a single rotational correlation time [28,29]. The short component (θ_1) is observed regardless of whether the labeled protein is in the native or denatured state or in the presence of ligands. In the absence of ligands, $\theta_2 = 288.7$ ns. The average of the two correlation times $\langle\theta\rangle = g_1\theta_1 + g_2\theta_2$ is 226 ns. This value is very similar to the single correlation time (220–250 ns) previously determined from time-domain data under comparable experimental conditions [28]. Since only a single correlation time was previously reported, it was concluded that the AEDANS probe attached to SH_1 was immobile. The present data do not allow us to establish unequivocally whether the short correlation time reflects probe motions or segmental motions of the protein. If it is associated with probe motions, the order parameter [30] of the probe is $S^2 = r_{02}/(r_{01} + r_{02}) = 0.776$, corresponding to a semiangle of 23.3° over which the probe dipole can traverse within a hypothetical cone. Because θ_1 is 9.5 ns, the probe motions are relatively slow. Ligands reduce the semiangle to the range of 11–19°, indicating that the probe motions are more restricted in the presence of bound ligand. The semiangle for MgADP + vanadate is the smallest.

The rotational correlation times of donor-labeled S1 are sensitive to ligands. In the presence of MgADP, θ_2 is reduced by 54% to 134 ns and $\langle\theta\rangle$ is decreased by 46% to 121 ns. These results differ from previous studies [28,29] which reported essentially identical correlation times for similarly labeled S1 in the absence and presence of MgADP. Addition of vanadate to S1·MgADP further reduces θ_2 to 93 ns, a 30% decrease. In a recent study, Aguirre et al. [31] reported a single rotational correlation time of 107 ns for native S1 complexed with Mg^{2+} and ϵADP, a value comparable to the present result obtained with labeled S1 in the presence of MgADP. Their study also reported a 30% decrease in the correlation time upon addition of V_i to S1·MgϵADP. Thus, the present findings obtained with labeled S1 corroborate the previous results obtained with native S1 [31]. After this manuscript was completed, an abstract appeared in which the rotational correlation coefficient of S1·MgADP was shown by electrical birefringence to decrease upon addition of vanadate [32], in qualitative agreement with our present and previous results [31].

We have recovered the distributions of FRET distances between extrinsic probes covalently linked to the thiols of Cys 697 and Cys 707 of the heavy chain of subfragment-1 by using frequency-domain data. For the calculations we assumed the distances to be Gaussian-distributed. This choice of the distribution function (eq. 19) is arbitrary at this time. We [11] recently showed that the recovered distributions for troponin I and several oligopeptides are each graphically very similar irrespective of the functional form of the distance distribution function, and similar results were obtained for S1 in the present case (results not shown). For these reasons we only reported the distributions in terms of eq. 19, instead of considering other functions which might be more appropriate for infinite polymeric chains [33].

The wide distributions which have been recovered cannot be easily explained by uncertainties in the orientation factor. Since no narrowing of $P(r)$ was observed for denatured S1, the observed hw for the native protein must, to a large extent, reflect an intrinsic distribution of the distances between the probes. The intrinsic distance distribution of any protein segment arises from protein conformational heterogeneity and dynamics and is determined by the primary as well as the secondary and tertiary structures of the protein segment. At this time we do not completely understand the effects of dynamics on the apparent distance distributions, but we expect donor-to-acceptor diffusion to decrease the width of the apparent distributions [15,34]. Upon denaturation the protein is expected to approach a

random coil and the segment in question exists in a large number of conformations. Consequently, in denatured protein the segment should exist in a wide range of donor-acceptor distances and the half width of the $P(r)$ should increase several-fold relative to native protein. This expectation has been confirmed in our recent studies of troponin I [11] and troponin C [35]. However, the observed increase of hw in the present case is only 45%. The absence of a large increase in hw upon denaturation of S1 suggests that the Cys 697-Cys 707 segment of the native protein is likely already in an overall conformation approaching that of a random coil and its fluctuation dynamics is not highly constrained. The small increase may be attributed to disruption of a weak secondary or tertiary structure upon denaturation. These results are direct physical evidence that the Cys 697-Cys 707 segment of S1 has an extraordinary flexibility comparable to a random coil. Recently, Huston et al. [36] reported that SH_1 and SH_2 were the primary residues cross-linked by either oxidation with 5,5′-dithiobis(2-nitrobenzoic acid) or treatment with *p*-phenylene-dimaleimide, and concluded that Cys 697 and Cys 707 can move toward each other by as much as 10 Å in the presence of nucleotide. Their finding is consistent with the observed shift of $P(r)$ under the influence of MgADP.

The amino acid sequence of S1 heavy chain from residues 694 to 718 is Gln(694)-Leu-Arg-Cys(697)-Asn-Gly-Val-Leu-Glu-Gly-Ile(704)-Arg-Ile-Cys(707)-Arg----Ala(718). On the basis of secondary structure prediction by the program PREDICT which combines seven separate methods, this segment of 25 residues appears to have no significant secondary structure except for the stretch of residues 704–708. The segment of residues 694–703 includes the thiol SH_1 of Cys 697. A sheet or reverse turn is indicated for the five residues Ile(704)-Arg-Ile-Cys(707)-Arg by four of the seven methods. Peptide segments between residues 694 and 703 and between 708 and 718 have little or no secondary structural constraint, but Cys 707 is relatively constrained within a sheet or turn structure. In the absence of bound nucleotide the thiol SH_2 of Cys 697 is not readily accessible to chemical modification. Under this condition, Cys 697 is likely shielded or structurally constrained from exposing itself to the protein surface. This constraint would make the residue relatively static. It would seem likely that certain structural elements within the segment containing Cys 697 and Cys 707 serve as flexible joint(s) to bring Cys 707 toward the relatively static Cys 697. In the presence of bound nucleotide the structural constraint imposed on Cys 697 is diminished, rendering its SH_2 accessible to chemical modification and allowing the two residues to come closer to each other by an average of 6–7 Å. This decrease of the mean separation is not accompanied by an appreciable change of the distribution half width. The effects of V_i and MgADP on $\bar{r}$ appear to be additive. The mean distance in the complex $S1 \cdot MgADP \cdot V_i$ is 10 Å smaller than in $S1 \cdot MgADP$, although their distribution widths differ by less than 2 Å.

The observed rotational correlation times have biological implications. In terms of the relationship between the contractile cycle and the intermediate states of myosin, the power stroke of the cycle occurs concomitantly with the release of phosphate [37] as a product of ATP hydrolysis. The power stroke begins with myosin states such as $A \cdot M \cdot ATP$ and $A \cdot M \cdot ADP \cdot P_i$, and ends with $A \cdot M \cdot ADP$ and $A \cdot M$ (where A is actin and M is the S1 moiety of myosin). The preferred orientation of S1 in $A \cdot M \cdot ADP \cdot P_i$ is usually taken as 90° and in $A \cdot M \cdot ADP$ as 45°. It has been suggested that there is a direct correspondence between the conformation of S1 in $A \cdot M \cdot ADP$ and $M \cdot ADP$ and that in $A \cdot M \cdot ADP \cdot P_i$ and $M \cdot ADP \cdot P_i$ [38]. Thus, the transition of myosin from $M \cdot ADP \cdot P_i$ to $M \cdot ADP$ would correspond to the power stroke. Since P_i has a very small affinity for M or $M \cdot ADP$, it is difficult to study the conformation of S1 in a state at or near the start of the power stroke. This difficulty can be circumvented by using the orthovanadate ion V_i to form the complex $M \cdot ADP \cdot V_i$ (or $S1 \cdot ADP \cdot V_i$) which is considered to be a good, stable analogue of $M \cdot ADP \cdot P_i$ (or $S1 \cdot ADP \cdot P_i$) [39]. The present work has taken advantage of this stable vanadate analogue. If S1 is approximated by a prolate ellipsoid of revolution, its two rotational correlation times (Θ_a and Θ_b) can be calculated from the

Perrin equation using appropriate frictional coefficients for different axial ratios γ [40]. For this purpose we use a partial specific volume of 0.720 ml g^{-1} for S1 [41] and assume water of hydration between 0.3 and 0.4 g water/g protein. The harmonic mean of Θ_a and Θ_b is in the range of 108–246 ns for $\gamma = 2$–5. When compared with these calculated harmonic means, the observed long correlation time Θ_2 of S1 suggests an axial ratio of about 4–5. The smaller values of Θ_2 for the S1 complexes are consistent with a decrease of γ to 2–3 for S1 · MgADP and to a value below 2 for S1 · MgADP · V_i. These smaller values could also be explained by a more flexible structure of S1 in the complexes. Taken together these results suggest considerable global perturbations of the S1 structure during its hydrolysis of ATP. The single rotational correlation time of a rigid spherical equivalent of S1 is in the range 60–90 ns with hydration from 0 to 0.4 g water/g protein. Thus, S1 · MgADP · V_i may have a hydrodynamic shape that is highly symmetric. Coupled with this hydrodynamic shape is a considerably smaller mean separation between SH_1 and SH_2 in the S1 · MgADP · V_i complex. These results provide a basis for suggesting a model in which myosin cross-bridges undergo conformational transitions from an elongated or relatively rigid structure to a compact or less rigid structure during its hydrolysis of ATP. Upon release of hydrolysis products, the cross-bridges return to a more elongated conformation. Since the putative elongation likely occurs at the end of the power stroke at which mechanical force is produced, this structural change can, at least in part, be responsible for development of contractile force. This mechanism would allow the S1 moiety of myosin to accommodate changes in interfilament spacing known to occur during contraction by changing its dimensions. The extent to which the transitions within S1 may be sufficient for this purpose is unclear at this time. This model differs from others in which contractile force is thought to be generated through rotational motions of the cross-bridges. These two types of structural changes, however, need not be mutually exclusive as components of an overall mechanism of energy transduction in muscle.

The ligand-induced decreases in the mean FRET distance likely reflect structural perturbations that are induced at the S1 active site and transmitted to other regions of the heavy chain, and do not seem to be accompanied by significant alteration of the dynamic fluctuations (distribution width) of the polypeptide segment between Cys 697 and Cys 707. Even in actin · S1, the hw is within 2 Å of that for other species. While the global perturbations identified here can be a component of the energy transduction mechanism, preservation of the dynamics of a short segment of the heavy chain in different myosin intermediate states may be an important structural feature for force generation. It is a working hypothesis [42] that a localized distortion of the S1 structure induced by formation of an enzymatic intermediate can be mechanically transmitted to the distant actin-myosin S1 interfaces. Such a transmission is thought to be a central part of the transduction mechanism. Structural dynamics provides a means by which transmission of reversible distortion of local structure can be facilitated. In a somewhat speculative fashion Botts et al. [42] have recently attempted to unify a number of structural and biochemical findings on S1 and discussed the requirement of structural flexibility within the S1 structure including that of the segment containing Cys 697 and Cys 707 for transmission of mechanical force in actomyosin. The extreme flexibility of the short segment between the two residues demonstrated in the present work may be a central structural feature that acts as a key transducer.

Acknowledgements

This work was supported by grants from the National Institutes of Health (AR 31239 to H.C.C. and GM 35154 to J.R.L.) and from the National Science Foundation (DMB-8804931 to J.R.L.), with support for instrumentation from the National Science Foundation (DMB-8511065) and the Center for Fluorescence Spectroscopy (DIR-8710401). J.R.L. and W.W. acknowledge support from the Medical Biotechnology Center at the University of Maryland.

References

1 M.F. Morales, J. Borejdo, J. Botts, R. Cooke, R.A. Mendelson and R. Takashi, Annu. Rev. Phys. Chem. 33 (1982) 319.
2 T. Hiratsuka, Biochemistry 26 (1987) 3168.
3 T. Sekine and W. Kielly, Biochim. Biophys. Acta 81 (1964) 336.
4 M. Yamaguchi and T. Sekine, J. Biochem. (Tokyo) 59 (1966) 24.
5 E. Reisler, M. Burke and W.F. Harrington, Biochemistry 83 (1974) 3837.
6 J.A. Wells and R.G. Yount, Proc. Natl. Acad. Sci. U.S.A. 76 (1979) 4966.
7 R.E. Dalbey, J. Weiel and R.G. Yount, Biochemistry 22 (1983) 4696.
8 H.C. Cheung, F. Gonsoulin and F. Garland, Biochim. Biophys. Acta 732 (1985) 52.
9 F. Garland, F. Gonsoulin and H.C. Cheung, J. Biol. Chem. 263 (1988) 11621.
10 J.R. Lakowicz, I. Gryczynski, H.C. Cheung, C.-K. Wang and M.L. Johnson, Biopolymers 27 (1988) 821.
11 J.R. Lakowicz, I. Gryczynski, H.C. Cheung, C.-K. Wang, M.L. Johnson and N. Joshi, Biochemistry 27 (1988) 9149.
12 J.R. Lakowicz, G. Laczko, H. Cherek, E. Gratton and M. Limkeman, Biophys. J. 46 (1984) 463.
13 P.R. Bevington, Data reduction and error analysis for the physical sciences (McGraw-Hill, New York, 1969) p. 242.
14 J.R. Lakowicz, G. Laczko and I. Gryczynski, Rev. Sci. Instrum. 57 (1986) 2499.
15 J.R. Lakowicz, W. Wiczk, I. Gryczynski, M. Sczmacinski and M.L. Johnson, Biophys. Chem., 38 (1990) 99.
16 B.P. Maliwal and J.R. Lakowicz, Biochim. Biophys. Acta 873 (1986) 161.
17 R. Aguirre, F. Gonsoulin and H.C. Cheung, Biochemistry 25 (1986) 6827.
18 A.G. Weeds and R.S. Taylor, Nature 257 (1975) 54.
19 J.A. Spudich and S. Watt, J. Biol. Chem. 246 (1971) 4866.
20 H.C. Cheung, F. Gonsoulin and F. Garland, J. Biol. Chem. 258 (1983) 5775.
21 P.D. Wagner and A.G. Weeds, J. Mol. Biol. 109 (1977) 455.
22 T.W. Houk and K. Ue, Anal. Biochem. 62 (1974) 66.
23 I. Gryczynski, W. Wiczk, M.L. Johnson and J.R. Lakowicz, Chem. Phys. Lett. 145 (1988) 436.
24 I. Gryczynski, W. Wiczk, M.L. Johnson, H.C. Cheung, C.-K. Wang and J.R. Lakowicz, Biophys. J. 54 (1988) 577.
25 S. Albaugh, J. Lan and R.F. Steiner, Biophys. Chem. 33 (1989) 71.
26 R.E. Dale, J. Eisinger and W.E. Blumberg, Biophys. J. 26 (1979) 161.
27 E. Haas, E. Katchalski-Katzir and I.Z. Steinberg, Biochemistry 17 (1978) 5064.
28 R.A. Mendelson, M.F. Morales and J. Botts, Biochemistry 12 (1973) 2250.
29 J. Botts, A. Muhlrad, R. Takashi and M.F. Morales, Biochemistry 21 (1982) 6903.
30 G. Lipari and A. Szabo, J. Am. Chem. Soc. 104 (1982) 4559.
31 R. Aguirre, S.-H. Lin, F. Gonsoulin, C.-K. Wang and H.C. Cheung, Biochemistry 28 (1989) 799.
32 S. Highsmith and D. Eden, Biophys. J. 57 (1990) 398a.
33 P.J. Flory, Statistical mechanics of chain molecules (Wiley, New York, 1969).
34 J.M. Beechem and E. Haas, Biophys. J. 55 (1989) 1225.
35 H.C. Cheung, C.-K. Wang, I. Gryczynski, G. Laczko, R.F. Steiner and J.R. Lakowicz, Biophys. J. 55 (1989) 122a.
36 E.E. Huston, J.C. Grammer and R.G. Yount, Biochemistry 27 (1988) 8945.
37 E. Eisenberg and L. Greene, Annu. Rev. Physiol. 42 (1980) 293.
38 J.W. Shriver and B.D. Sykes, Biochemistry 20 (1981) 2004.
39 R.S. Goody, W. Hoffman, M.K. Reedy, A. Magid and C. Goodno, J. Muscle Res. Cell Motil. 1 (1980) 198.
40 S. Koenig, Biopolymers 14 (1975) 2921.
41 S.S. Margossian and S. Lowey, Methods Enzymol. 85 (1982) 55.
42 J. Botts, J.F. Thomason and M.F. Morales, Proc. Natl. Acad. Sci. U.S.A. 86 (1989) 2204.